ELSEVIER

Journal of Fluids and Structures 24 (2008) 366–381

JOURNAL OF FLUIDS AND STRUCTURES

www.elsevier.com/locate/jfs

Unsteady separated and reattaching turbulent flow over a two-dimensional square rib

Y.Z. Liu[a,*], F. Ke[a], H.J. Sung[b]

[a]*School of Mechanical Engineering, Shanghai Jiao Tong University, 800, Dongchuan Road, Minhang District, Shanghai 200240, China*
[b]*Department of Mechanical Engineering, Korea Advanced Institute of Science and Technology, 373-1, Guseong-dong Yuseong-gu, Daejeon 305 701, South Korea*

Received 19 September 2006; accepted 22 August 2007
Available online 20 February 2008

Abstract

The spatio-temporal characteristics of the separated and reattaching turbulent flow over a two-dimensional square rib were studied experimentally. Synchronized measurements of wall-pressure fluctuations and velocity fluctuations were made using a microphone array and a split-fiber film, respectively. Profiles of time-averaged streamwise velocity and wall-pressure fluctuations showed that the shear layer separated from the leading edge of the rib sweeps past the rib and directly reattaches on the bottom wall ($x/H = 9.75$) downstream of the rib. A thin region of reverse flow was formed above the rib. The shedding large-scale vortical structures ($fH/U_0 = 0.03$) and the flapping separation bubble ($fH/U_0 = 0.0075$) could be discerned in the wall-pressure spectra. A multi-resolution analysis based on the maximum overlap discrete wavelet transform (MODWT) was performed to extract the intermittent events associated with the shedding large-scale vortical structures and the flapping separation bubble. The convective dynamics of the large-scale vortical structures were analyzed in terms of the autocorrelation of the continuous wavelet-transformed wall pressure, cross-correlation of the wall-pressure fluctuations, and the cross-correlation between the wall pressure at the time-averaged reattachment point and the streamwise velocity field. The convection speeds of the large-scale vortical structures before and after the reattachment point were $U_c = 0.35U_0$ and $0.45U_0$, respectively. The flapping motion of the separation bubble was analyzed in terms of the conditionally averaged reverse-flow intermittency near the wall region. The instantaneous reattachment point in response to the flapping motion was obtained; these findings established that the reattachment zone was a $1.2H$-long region centered at $x/H = 9.75$. The reverse-flow intermittency in one period of the flapping motion demonstrated that the thin reverse flow above the rib is influenced by the flapping motion of the separation bubble behind the rib.

Keywords: Separated and reattaching turbulent flow; Surface-mounted rib; Wall-pressure fluctuations; Large-scale vortical structures; Flapping motion

1. Introduction

Surface-mounted ribs are used to enhance turbulent heat transfer in various industrial applications (Acharya et al., 1994), such as gas turbines (Saha and Acharya, 2005), heat exchangers (Panigrahi and Acharya, 2004), and combustion

*Corresponding author. Tel.: +86 21 6293 2885; fax: +86 21 6447 0679.
E-mail address: yzliu@sjtu.edu.cn (Y.Z. Liu).

0889-9746/$ - see front matter © 2007 Elsevier Ltd. All rights reserved.
doi:10.1016/j.jfluidstructs.2007.08.009

Nomenclature

a	timescale dilation parameter (s)
b	time translation parameter (s)
B	streamwise rib width (m)
c_P	wall static pressure coefficient, $c_P = p/0.5\rho U_0^2$
$c_{P'}$	wall-pressure fluctuation coefficient, $c_{P'} = p'_{\mathrm{rms}}/0.5\rho U_0^2$
D	detailed part of the wavelet transformed signal
f	frequency (Hz)
$G_{p'p'}$	wall-pressure autospectrum (dB)
H	rib height (m)
p	wall static pressure (Pa)
p'	fluctuating part of the wall pressure (Pa)
p'_{rms}	root-mean-square of pressure fluctuations (Pa)
Re_H	Reynolds number based on the rib height
Re_θ	Reynolds number based on the momentum thickness
S	smooth part of the wavelet transformed signal
t	time (s)
T	shedding period of the large-scale vortical structures (s)
u	time-averaged streamwise velocity ($\mathrm{m\,s^{-1}}$)
u'	fluctuation part of the streamwise velocity ($\mathrm{m\,s^{-1}}$)
u'_{rms}	root-mean-square of the streamwise velocity fluctuation ($\mathrm{m\,s^{-1}}$)
U_0	free stream velocity ($\mathrm{m\,s^{-1}}$)
U_c	convection velocity ($\mathrm{m\,s^{-1}}$)
x	streamwise coordinate (m)
x_0	streamwise coordinate of the reference point (m)
x_R	reattachment length of the separation bubble behind the rib (m)
y	lateral coordinate (m)
$wf(b,a)$	continuous wavelet transform coefficient
$wc(a,\tau)$	wavelet autocorrelation function

Greek symbols

γ_t	reverse-flow intermittency factor
δ	boundary layer thickness (m)
δ^*	displacement thickness (m)
θ	momentum thickness (m)
ξ	streamwise separation interval (m)
$\rho_{pp}(\xi,\tau;x_0)$	space-time cross-correlation coefficient
$\rho_{pu}(x,y,\tau)$	cross-correlation coefficient of wall-pressure and streamwise velocity component
τ	time delay (s)
$\psi(t)$	mother wavelet
ω	angular frequency ($\mathrm{rad\,s^{-1}}$)

Abbreviations

MODWT	Maximum Overlap Discrete Wavelet Transform
MRA	Multi-Resolution Analysis
PXI	PCI eXtensions for Instrumentation

ducts (Hwang et al., 1999). The movement of a turbulent boundary layer flow over a surface-mounted rib gives rise to a strongly separated and reattaching flow. Previous studies of turbulent flows over forward- and backward-facing steps (Eaton and Johnston, 1981; Chun et al., 2004; Liu et al., 2005) and a fence (Hudy et al., 2003) established that strongly unsteady behaviors, such as rolled-up vortices, the shedding large-scale vortical structures, and a flapping separation bubble, are inherent in the separated and reattaching flow. However, the flow over a surface-mounted rib was found to exhibit a combination of the features observed in turbulent flows over forward- and backward-facing steps (Bergeles and Athanassiadis, 1983), including complex unsteady characteristics of the separated and reattaching flow. The unsteady behaviors of the separated and reattaching turbulent flow over a surface-mounted rib (Panigrahi and Acharya, 1996) significantly modulate its flow and heat transfer performance.

Numerous studies have sought to understand the separated and reattaching turbulent flow over a surface-mounted rectangular rib (Tropea and Gackstatter, 1985; Hwang et al., 1999; Panigrahi and Acharya, 2004). The time-averaged lengths of the recirculation regions before and behind the rib were found to depend on the ratio of the boundary layer thickness (δ) of the approaching flow to the rib height (H) and the ratio of the streamwise rib width (B) to the rib height (Antoniou and Bergeles, 1988; Hwang et al., 1999). Castro (1979) and Acharya et al. (1994) measured the profiles of mean velocity, shear stress and turbulence intensity of the relaxing wake downstream of a surface-mounted rib. Bergeles and Athanassiadis (1983) and Hwang et al. (1999) reported the length of the recirculation region (x_R) behind a two-dimensional surface-mounted rib as a function of B/H for the flow configurations $\delta/H = 0.48$ and 3.3, respectively. When B/H is larger than 4, the shear layer separated from the leading edge, subsequently reattaches on the top surface of the rib and then the downstream bottom wall; in these systems, the recirculation length (x_R) of the separation bubble behind the rib is almost independent of the streamwise rib width. When B/H is less than 4, in contrast, the shear layer sweeps past the rib and directly reattaches on the downstream bottom wall of the rib, while x_R decreases linearly with increasing the streamwise rib width (Bergeles and Athanassiadis, 1983; Hwang et al., 1999). The separated and

reattaching flow over a square rib ($B/H = 1.0$) has received widespread attention due to its complex turbulence behavior (Acharya et al., 1994; Panigrahi and Acharya, 1996, 2004) and its potential uses in industrial applications (Murata and Mochizuki, 2000; Saha and Acharya, 2005). Acharya et al. (1994) found that the turbulence was far from equilibrium in the recirculation and shear layer regions, and that non-equilibrium conditions still persisted at 7 rib heights downstream of the reattachment zone ($x_R/H = 6.3 \pm 0.9$). Panigrahi and Acharya (1996) surveyed velocity spectra of the separated flow behind a surface-mounted square rib by varying the free-stream velocity and the rib size while keeping $B/H = 1.0$. They found that the shedding frequency of large-scale vortical structures increased linearly with increasing Reynolds number, but was almost invariant with respect to rib size. More recently, the same authors examined the influence of acoustic excitation on the production and transport of coherent turbulent structures in the flow over a surface-mounted square rib using auto-correlation and quadrant analysis of the velocity data (Panigrahi and Acharya, 2004). Their results showed the dominant presence of the large-scale vortical structures in the redeveloping turbulent boundary layer.

The main objective of the present study was to elucidate the unsteady behavior of the separated and reattaching turbulent flow over a two-dimensional square rib ($B/H = 1.0$) flush mounted on the wall. To this end, a joint measurement system consisting of a synchronized split-fiber film probe and microphone array was established with a view of simultaneously surveying velocity fluctuations and wall-pressure fluctuations, respectively. Wall-pressure fluctuations, which are regarded as signatures of vortices convecting over the wall (Farabee and Casarella, 1986; Chun et al., 2004; Liu et al., 2005), were analyzed to quantify the dynamics of the vortical structures and the separation bubble in the separated and reattaching turbulent flow. The flow was analyzed in terms of profiles of the time-averaged streamwise velocity, wall static pressure distribution, wall-pressure fluctuation coefficient, wall-pressure spectra, and the cross-correlation of the wall pressure and velocity field. Flapping of the separation bubble was examined in terms of the conditionally averaged reverse-flow intermittency in the near-wall region.

2. Experimental apparatus

Experiments were performed in the subsonic open-circuit wind tunnel employed previously by Liu et al. (2006, 2007). A honeycomb and five screens were placed in sequence in the settling chamber. A diffuser and a smooth contraction fairing with a contraction ratio of 6:1 ensured high-quality flows in the test-section. The dimensions of the inlet channel were 300 mm (width) × 300 mm (height) × 1000 mm (length). Air was driven by a centrifugal blower and a 1.5 kW motor. The test-section was $300 \times 300\,\text{mm}^2$ in cross-section and 2000 mm in length. The speed of the flow in the test-section was controlled using an inverter (Danfoss, Denmark). For the range of flow velocities considered (5–20 m s^{-1}), the free-stream turbulence intensity was less than 0.8% and the potential core was uniform within 0.6% in the spanwise and vertical directions. No significant peaks were observed in the spectrum of velocity fluctuations in the main flow. As shown in Fig. 1, a 1500 mm long false floor was installed 40 mm above the bottom wall of the test section; a slight skew angle (15°) was machined at the bottom side of its leading edge to suppress distortion of the free stream by the false floor. A two-dimensional square rib with streamwise rib width $B = 20$ mm and height $H = 20$ mm was flush-mounted 400 mm downstream of the leading edge. Given that the aspect ratio was larger than 12, the turbulent flow over the rib was assumed to be two-dimensional along the centerline (Brederode and Bradshaw, 1978; Roos and Kegelman, 1986; Panigrahi and Acharya, 1996). To achieve a fully developed turbulent boundary layer flow, a trip wire and a 20 mm wide strip of sandpaper were attached to the entrance wall of the false floor. The total blockage ratio of the test section due to the rib and the false floor was 8.3%. The inlet free-stream velocity was fixed at $U_0 = 10\,\text{m s}^{-1}$, resulting in a Reynolds number based on the rib height of $\text{Re}_H = 13\,200$. The boundary layer thickness δ, displacement thickness δ^*, and momentum thickness θ of the turbulent boundary layer at the rib position in the absence of the rib were 15.0, 2.2, and 1.7 mm, respectively. The shape factor of the boundary layer was 1.3. The Reynolds number based on the momentum thickness Re_θ was 1130. The ratio of the boundary layer thickness to the rib height was $\delta/H = 0.75$, indicating that the rib will strongly disturb the flow.

The standard hot-wire technique was used with a constant temperature anemometer (Streamline, Dantec Inc., Denmark). Profiles of the time-averaged streamwise velocity of the turbulent boundary layer at the rib position in the absence of the rib were measured using a single-wire probe (55P11, Dantec Inc., Denmark). A split-fiber film probe (55R55, Dantec Inc., Denmark) was employed to survey the turbulence properties of the separated and reattaching turbulent flow. The probe operated at an overheat ratio of 1.8 was calibrated online by a commercial nozzle facility (90H10, Dantec Inc., Denmark) integrating a settling chamber, a set of control valves, and pressure and temperature transducers. The calibration was performed in relation to the magnitude and yaw angle of the determined velocity. In the experiments, all the single-point measurements were taken along the mid-span of the tunnel. Forty-seven

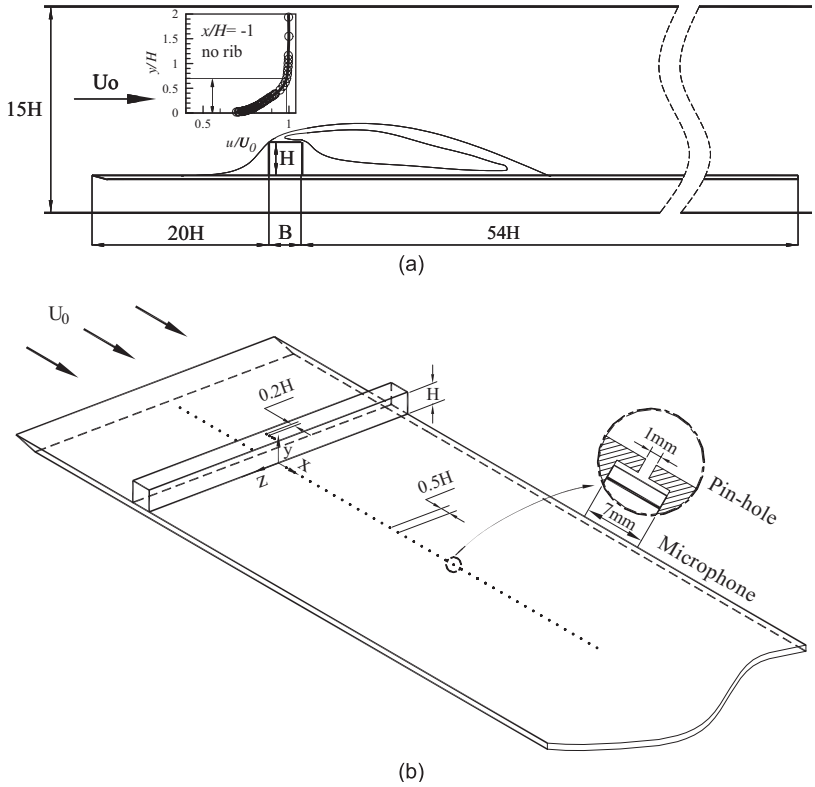

Fig. 1. Schematic diagram of the experimental set-up.

measurement stations, separated by intervals of $0.5H$ upstream and downstream of the rib and intervals of $0.2H$ on top of the rib, were defined along the streamwise direction. In the wall-normal direction, 41 measurement points were distributed nonuniformly in the region $y/H \leqslant 6.0$. The sampling frequency was 5 kHz and a total of 409 600 voltage signals were acquired at each measurement point. The accuracy of the velocity values obtained using the split-fiber film probe was within 1% for the velocity range considered in the present study. The frequency response characteristics of the probe were found to be flat below 15 kHz by a square-wave test.

As shown in Fig. 1, a total of 34 ICP-type microphones (G.R.A.S., 40PQ, Denmark), which have a wide dynamic range of 30–138 dB, were installed on the perforated plate and rib to capture wall-pressure signatures of the convecting vortices buried in the separated and reattaching flow (Lee and Sung, 2002). In the streamwise direction, four wall-pressure measurement stations beginning at $x/H = -0.8$ were arranged on the top surface of the rib at intervals of $0.2H$; downstream of the rib, 30 wall-pressure measurement stations beginning at $x/H = 0.25$ were arranged on the bottom wall at intervals of $0.5H$. To increase the spatial and frequency resolution of each microphone, a pinhole of diameter 1 mm and an installation cavity of diameter 7.0 mm were drilled concentrically on the bottom plate at each measurement station (Liu et al., 2005, 2006). In an effort to accurately estimate the spectral energy distribution, each microphone was calibrated against a piston phone (PCB 394A40, USA) and a half-inch reference microphone (G.R.A.S. 40AE, Denmark) in a calibrator, yielding specific frequency-magnitude and frequency-phase relationships for each microphone (Lee and Sung, 2002); typically, the sensitivity of the microphones was about 7.7–8.2 mV/Pa. In the frequency region of the present study, the magnitude error and phase delay of the microphones were within ± 1 dB and $\pm 3^\circ$, respectively. In the experiments, the time-series wall-pressure data were reconstructed in the frequency/phase domain (Chun et al., 2004; Lee and Sung, 2002). The wide dynamic range of the microphones (30–138 dB) guaranteed high levels of measurement accuracy without applying any further compensation procedure to the output of the arrayed microphones (Lee and Sung, 2002). To exclude data scatter associated with uncertainties in the microphone calibration procedure (Hudy et al., 2003), sequential measurements of the wall-pressure fluctuations were performed using a single microphone to obtain wall-pressure fluctuation coefficients and wall-pressure spectra along the streamwise direction. The uncertainty in the pressure measurement was estimated to be $\pm 3\%$. Simultaneous acquisition of the wall-pressure fluctuation signals at the sampling frequency of 5 kHz was performed using LabVIEW software and a data acquisition

system (NI4472B/PXI-1042Q, NI Inc., USA). The cut-off frequency for measuring the wall-pressure fluctuations was fixed at 2.2 kHz. A total of 409 600 time series data were acquired for each microphone. Thus, the time period over which the wall-pressure fluctuations were measured encompassed around 1200 and 4800 intermittent events of the shedding large-scale vortical structures ($fH/U_0 = 0.03$) and flapping separation bubble ($fH/U_0 = 0.0075$), respectively.

In the experiments, acquisition of the wall-pressure fluctuations using the microphone array was synchronized with that of the velocity fluctuations using the split-fiber film probe. When the velocity fluctuations at each point (over 1900 measurement points in total) were sampled, the instantaneous wall-pressure fluctuations in the range of $-0.8 \leqslant x/H \leqslant 15.0$ were obtained simultaneously, resulting in over 750 GB of experimental data. A real-time PXI chassis (PXI-1042Q, NI Inc., USA), which was installed with six dynamic signal acquisition cards (PXI-4472B, NI Inc., USA) and communicated with the personal computer through a fiber cable, was used to synchronize sampling of the fluctuating signals from the microphone array (34 channels) and the split-fiber film probe (2 channels). Furthermore, in the synchronized acquisition of the signals from these 36 channels, the inter-channel time delay was less than 0.3 μs, which corresponded to around 4.5×10^{-6} of the shedding period of the large-scale vortical structures and was three orders of magnitude smaller than the period of the highest frequency (2 kHz) examined in the present study. This enabled reliable simultaneous acquisition of the wall-pressure fluctuations and the velocity fluctuations.

Finally, the pinholes used for measuring the wall-pressure fluctuations were adapted for installing static pressure taps, which were connected to a 16-channel Scanivalve (DSA3017, Scanivalve, USA) with 0.1% accuracy. A total of 5000 samples were acquired at 45 Hz at each measurement station; the duration of data acquisition covered over 1600 and 6400 intermittent events of the shedding large-scale vortical structures and flapping separation bubble, respectively. Thus, the variation of wall static pressure due to unsteady behavior buried in the separated and reattaching flow was effectively eliminated, yielding a reliable time-averaged static pressure.

3. Results and discussion

A schematic diagram of the flow configuration is shown in Fig. 1(b). Unlike the flow over a large-width rib ($B/H > 4$), the turbulent flow separated from the leading edge of the square rib ($B/H = 1$) sweeps past the rib and directly reattaches on the bottom wall downstream of the rib (Bergeles and Athanassiadis, 1983). Before examining the unsteady characteristics of the separated and reattaching turbulent flow, we first examined the profiles of time-averaged streamwise velocity across the area ($-4 \leqslant x/H \leqslant 15.75$, $0 \leqslant y/H \leqslant 6$) (Fig. 2). The approaching flow separates from the wall at $x/H = -2$ due to blockage by the rib, forming a separated zone $2H$ in length upstream of the rib. At the leading edge of the rib ($x/H = -1$), the flow is immediately separated and a thin layer of reversed flow forms above the rib. The presence of reversed flow at $x/H = 0$ confirms that the flow separated from the leading edge of the rib does not reattach on the rib surface (Bergeles and Athanassiadis, 1983). The difference in the vertical extent of the reverse flow zone at the stations at $x/H = -0.6$ and 0 indicates the growth of the reversed flow before being relaxed downstream of the rib, which may have a significant influence on the separated and reattaching turbulent flow behind the rib. Subsequently, the turbulent flow expands downstream of the rib and a slender recirculation zone is formed behind the rib. At $x/H = 9.75$, the turbulent shear layer reattaches to the bottom wall and relaxes into a redeveloping turbulent boundary layer. However, the streamwise velocity component is not fully recovered even at $x/H = 15.75$, which is attributed to the slow decay of the large-scale vortical structures in the redeveloping turbulent boundary layer (Panigrahi and Acharya, 2004; Liu et al., 2005). Furthermore, as seen in Table 1, the recirculation zone behind the square rib is considerably larger than those behind forward- and backward-facing steps (Farabee and Casarella, 1986), demonstrating the strong perturbation of the turbulent boundary layer by the square rib.

Fig. 3 shows profiles of the time-averaged streamwise velocity fluctuation intensity (u'_{rms}/U_0) at various streamwise locations. The velocity fluctuations are more intense along the dividing streamline beginning from the leading edge of the rib. The velocity fluctuations reach their highest level ($u'_{rms}/U_0 = 18\%$) at $x/H = 0$ and $y/H = 1.2$. As the vortices begin to emanate from the thin reversed flow above the rib, the zone of large fluctuations immediately grows in size ($x/H = 0.75$) and the fluctuating amplitude slowly diminishes, demonstrating the influence of the growing large-scale vortical structures ($0.75 \leqslant x/H \leqslant 9.75$). At the reattachment position ($x/H = 9.75$) of the separated flow, the fluctuating amplitude is kept at $u'_{rms}/U_0 = 16\%$ over a large wall-normal area ($1H$). After the flow reattaches to the wall, the zone of large fluctuations flattens out due to the strong interaction between the large-scale vortical structures and the wall. Near $x/H = 15.75$ ($(x-x_R)/x_R = 0.62$), the streamwise velocity fluctuations are attenuated to $u'_{rms}/U_0 = 14\%$ due to the decay of the large-scale vortical structures. In the separated and reattaching flow over a backward-facing step (Chun et al., 2004; see Table 1), by comparison, the peak of streamwise velocity fluctuations is reduced from 18% to 13% on going from the reattachment point ($x_R/H = 6.11$) to the position ($(x-x_R)/x_R = 0.67$. Thus, the slower reduction of the

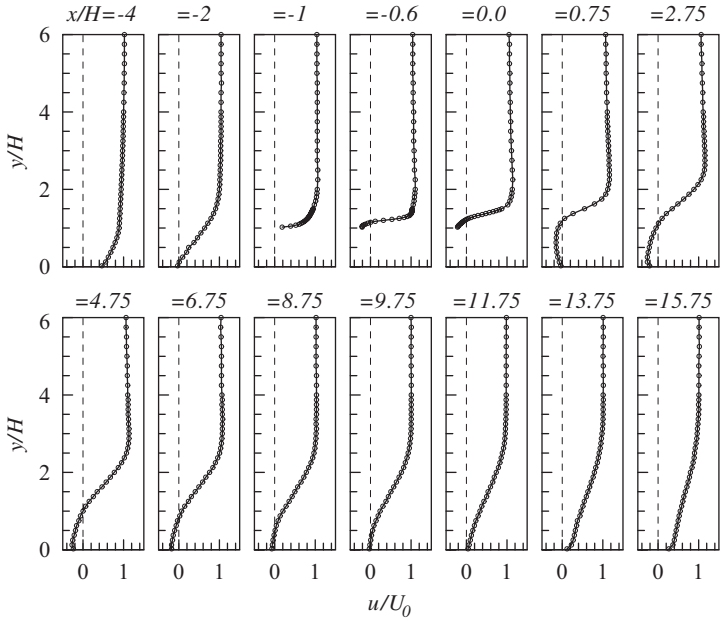

Fig. 2. Profiles of time-averaged streamwise velocity.

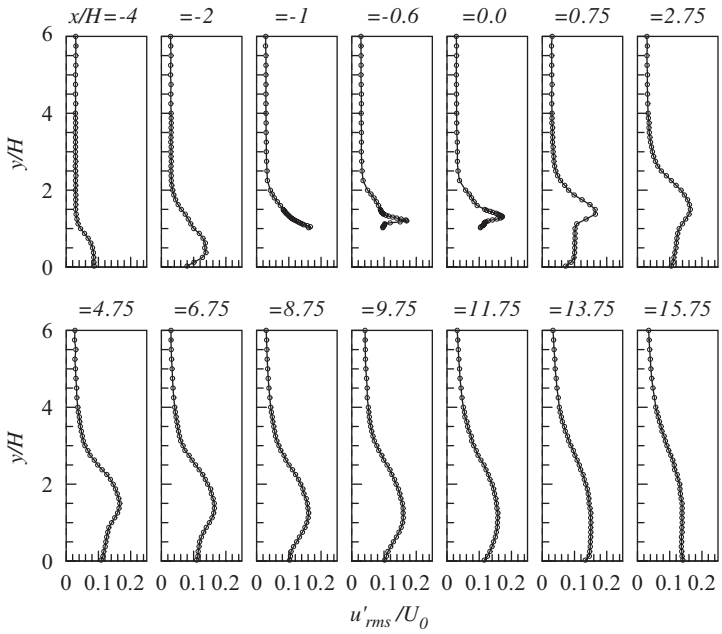

Fig. 3. Profiles of time-averaged streamwise velocity fluctuation intensity.

streamwise velocity fluctuations observed in the present study indicates that the decay rate of the large-scale vortical structures in the redeveloping boundary layer behind the square rib is slower than that of the large-scale vortical structures behind the backward-facing step (Chun et al., 2004). To delineate the trail of the convecting vortices in the separated and reattaching turbulent flow, we examined the wall-normal positions of the local maximum streamwise velocity fluctuations as a function of streamwise position (Fig. 4). The maximum streamwise velocity fluctuations occur at $y/H = 1.2$ when $x/H \leqslant 6$. As the flow goes downstream from $x/H = 6$, the location in the wall-normal direction at which the streamwise velocity fluctuations are most intense moves slightly toward the wall. The gradual decrease in the

Table 1
Summary of the present and previous data for separated and reattaching flows over surface irregularities

References	Configuration	H (mm)	U_0 (m/s)	δ/H	x_R/H	(U_c, $(x-x_R)/x_R$)
Farabee and Casarella (1986)	Backward-facing step	12.7	26.8	1.0	6–8	($\approx 0.2U_0$, −0.67) ($\approx 0.4U_0$, 0)
Farabee and Casarella (1986)	Forward-facing step	12.7	24.7	2.4	3–4	($\approx 0.4U_0$, −0.5) ($\approx 0.55U_0$, 0)
Heenan and Morrison (1998)	Backward-facing step	75	34.5	0.32	5.5	($\approx 0.38U_0$, −0.41) ($\approx 0.5U_0$, 0)
Hudy et al. (2003)	Fence	7.9	15	–	25.6	($0.2U_0$, −0.74) ($0.57U_0U_0$, 0)
Chun and Sung (1996)	Backward-facing step	50	4	0.28	6.75	–
Chun et al. (2004)	Backward-facing step	50	10	0.49	6.11	($0.52U_0$, 0)
Liu et al. (2005)	Backward-facing step	50	10	0.4	7.75	($0.56U_0$, 0)
Antoniou and Bergeles (1988)	Square rib	20	15	0.7	10	–
Bergeles and Athanassiadis (1983)	Square rib	25	16	0.48	−11.5	–
Present study	Square rib	20	10	0.75	9.75	($0.35U_0$, −0.51) ($0.45U_0$, 0)

position of maximum fluctuations over the range $9.75 \leqslant x/H \leqslant 12.0$ indicates the persistence of the large-scale vortical structures in the redeveloping turbulent boundary layer. Beyond $x/H > 12$, the position of maximum fluctuations shifts more rapidly toward the wall, due to the decay of the vortical structures under the influence of the wall (Wood and Bradshaw, 1982; Liu et al., 2006).

To more closely inspect the near-wall reverse flow behavior, we examined the time-averaged streamwise velocity close to the wall ($y/H = 0.05$) (Fig. 5). The streamwise variation of the reverse-flow intermittency factor (γ_t) is also included in Fig. 5 for comparison. In the near-wall region, the reversed flow reaches a maximum streamwise velocity of $u/U_0 = -0.25$ at $x/H = 4$. The streamwise position at which $\gamma_t = 0.5$ exactly corresponds to the time-averaged reattachment point at $x/H = 9.75$. The sharp variation of γ_t near the reattachment point can be attributed to the complex interaction between the reattaching large-scale vortical structures and the flapping separation bubble (Lee and Sung, 2002; Chun et al., 2004), whereas the large variation of γ_t in the region $6 \leqslant x/H \leqslant 14$ can be attributed to the flapping motion of the separation bubble (Liu et al., 2005). In the region far downstream of the rib ($x/H \geqslant 14.75$), the near-wall region is immune to the influence of the flapping separation bubble, and hence the intermittency factor is $\gamma_t \equiv 0$. However, in the region far upstream of the reattachment point ($x/H < 6$), the intermittency factor γ_t deviates from the value of 1 expected for the fully reversed flow, which may be due to the intermittent enlargement motion of the separation bubble (Lee and Sung, 2002).

Fig. 6 shows the streamwise distribution of the wall static pressure, which was measured relative to the wall static pressure at $x/H = -4.25$. As shown in Fig. 6, the blockage of the approaching flow by the rib gives rise to a gradual increase in wall static pressure upstream of the leading edge, followed by a sudden drop in wall static pressure immediately downstream of the leading edge. On top of the rib, the wall static pressure increases rapidly due to the reversed flow. In the region downstream of the rib ($x/H < 4.0$), however, the wall static pressure gradually decreases; this decrease reflects the elevation of the separated shear layer observed in Fig. 4. On moving beyond $x/H < 4.0$, the wall static pressure slowly increases due to the convergence of the time-mean dividing streamline directed toward the wall at $x/H = 9.75$. After the reattachment of the large-scale vortical structures to the wall, the recovery of the wall static pressure progresses in the redeveloping turbulent boundary layer.

As mentioned above, the wall-pressure fluctuations felt by a wall over which a fluid is flowing are closely related to the instantaneous motions of the vortices buried in the shear layer, and hence can be looked upon as the footprints of the vortices convecting over the wall (Lee and Sung, 2002). To take advantage of this characteristic, we measured the wall-pressure fluctuations at 63 streamwise stations ($-4.25 \leqslant x/H \leqslant 24.75$) using a single microphone. Fig. 7 shows the streamwise distribution of the wall-pressure fluctuation coefficient normalized by the free-stream velocity head. For comparison, the streamwise distribution of the wall-pressure fluctuation coefficient for the separated and reattaching flow over a backward-facing step reported by Chun et al. (2004) are included. Over the coverage of the rib surface the abrupt increase in the amplitude of the wall-pressure fluctuations continues until the fluid flows beyond the rib, which is a reflection of the fact that the flow separated from the leading edge does not reattach on the top surface of the rib (Liu et al., 2005). Immediately behind the rib the wall-pressure fluctuations are significantly reduced due to the corner flow and the spatially filtered influence of the convecting vortices at a large distance ($1H$) above the bottom wall. Further downstream, the growing vortical structures embedded in the separated and reattaching flow intensify the wall-pressure fluctuations, which reach a maximum near the reattachment point ($x/H = 9.75$). Close inspection of the wall-pressure fluctuation coefficients behind the reattachment points discloses that $c_{P'}$ for the flow over the rib decreases more slowly than that for the separated and reattaching flow over a backward-facing step (Chun et al., 2004). This slower decrease in

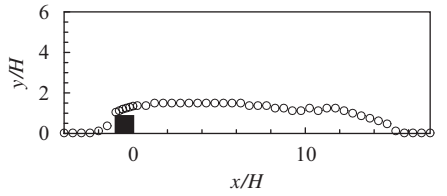

Fig. 4. Wall-normal location for maximum streamwise velocity fluctuations.

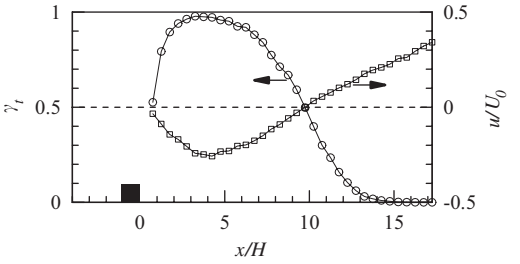

Fig. 5. Distribution of reverse-flow intermittency and time-averaged streamwise velocity measured at the height $y/H = 0.05$.

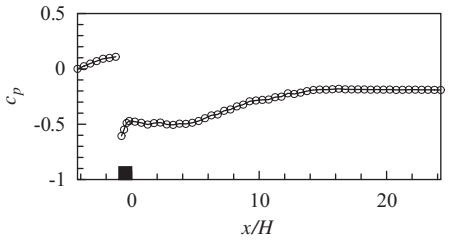

Fig. 6. Wall static pressure distribution ($c_P = p/0.5\rho U_0^2$).

$c_{P'}$ reflects the persistence of the large-scale vortical structures in the redeveloping turbulent boundary layer downstream of the rib (Panigrahi and Acharya, 2004). In the classic separated and reattaching flows over backward- and forward-facing steps, the peak value of the wall-pressure fluctuations at the reattachment point of the forward-facing step was larger than that at the reattachment point of the backward-facing step (Farabee and Casarella, 1986). However, for the separated and reattaching flow over a square rib, which comprises a forward-facing followed by backward-facing step, the peak value of the wall-pressure fluctuations on the top surface of the rib is slightly lower than that near the reattachment point ($x/H = 9.75$) behind the rib. This discrepancy can be attributed to the fact that the separated shear layer does not reattach to the top surface of the rib.

To further examine the contribution of the various-sized vortices to the wall-pressure fluctuations, we measured the wall-pressure autospectra at various streamwise stations (Fig. 8). For all locations downstream of the rib, the spectral magnitude peaked near $fH/U_0 = 0.03$, which is assigned to the shedding of the energetic large-scale vortical structures. On the top surface of the rib ($x/H = -0.2$), two prominent peaks are observed, at $fH/U_0 = 0.03$ and 0.12. The low frequency peak ($fH/U_0 = 0.03$) can be attributed to the global influence of the large-scale vortical structures shedding in the elevated shear layer. The peak at $fH/U_0 = 0.12$, which corresponds to the second harmonic frequency, indicates the amalgamation of the rolled-up vortices emanating from the leading edge. The lack of a peak at the first harmonic frequency ($fH/U_0 = 0.06$) may be due to the use of insufficient microphones to adequately cover the top surface of the rib. The wall-pressure fluctuations in the low-frequency range are markedly stronger at the reattachment point $x/H = 9.75$, where the spectrum exhibits a peak at $fH/U_0 = 0.03$ due to the reattachment of the large-scale vortical structures on the wall. Downstream of the reattachment point, the high-frequency spectrum at $x/H = 13.75$ exceeds that at $x/H = 9.75$ due to the decay of the large-scale vortical structures in the redeveloping turbulent boundary layer (Liu et al., 2005). Correspondingly, on going from $x/H = 9.75$ to 13.75, the peak spectrum amplitude migrates to higher frequency, as shown in Fig. 8. The streamwise variation of the low-frequency spectrum downstream of the rib

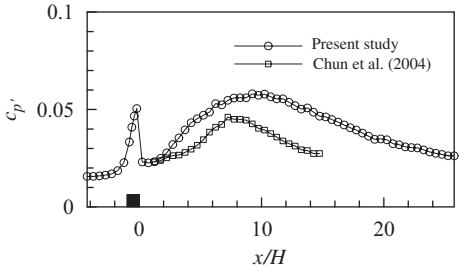

Fig. 7. Wall-pressure fluctuation coefficient ($c_{P'} = p'_{\mathrm{rms}}/0.5\rho U_0^2$).

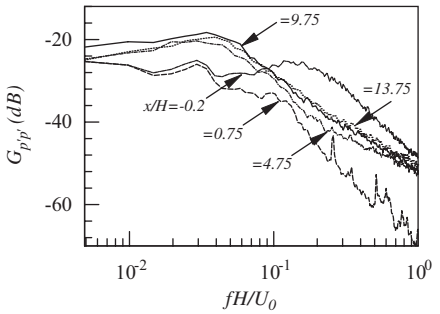

Fig. 8. Wall-pressure spectrum.

demonstrates that the strength of the spectrum near $fH/U_0 = 0.0075$ increases with increasing x/H, reaching a maximum at the reattachment point ($x/H = 9.75$), then decreasing on going further downstream. This prominent spatial variation in the strength of the low-frequency spectrum, which has previously been documented in studies of the separated and reattaching flow over a backward-facing step (Lee and Sung, 2002; Liu et al., 2005), corresponds to the flapping motion of the separation bubble behind the rib.

To resolve the correlative characteristics of the vortical structures at various scales, a wavelet autocorrelation analysis (Li, 1998) in terms of local frequency and time delay was performed on the wall-pressure fluctuation data. Based on the Mexican hat wavelet $\psi(t) = (1 - t^2)\exp(-\frac{1}{2}t^2)$, the continuous wavelet transform coefficient of a real-time series of data $f(t)$ is defined as

$$wf(b,a) = \frac{1}{a}\int_{-\infty}^{+\infty} f(t)\psi\left(\frac{t-b}{a}\right)\mathrm{d}t, \tag{1}$$

where a is the timescale dilation parameter and b is the time transition parameter. The wavelet autocorrelation function, $wc(a,\tau)$, is given by

$$wc(a,\tau) = \lim_{T\to\infty}\frac{1}{T}\int_{-T/2}^{T/2} wf(b,a)wf(b+\tau,a)\,\mathrm{d}t, \tag{2}$$

where τ is the time delay of the wavelet coefficients in wavelet space. Fig. 9 depicts the wavelet autocorrelation coefficients of the wall pressure at $x/H = -0.2$, 0.75, 4.75 and 9.75. According to the conversion formula $f = \sqrt{2.5}/2\pi a$ (Lee and Sung, 2002), the dashed line along $\log(aU_0/H) = 0.092$ denotes $fH/U_0 = 0.03$, which is assigned to the shedding frequency of the large-scale vortical structures. Obviously, the high-correlation zones along the $\tau U_0/H$ coordinate indicate that subsequently passing vortical structures are similar to previous ones. At the location $x/H = 9.75$, where the energetic large-scale vortical structures come into contact with the wall, six high-correlation zones are observed, at $\tau U_0/H = 0$, 30, 55, 90, 115 and 170. This indicates that six highly correlated convecting vortical structures successively pass the location $x/H = 9.75$, intensifying the local wall-pressure fluctuations. A similar pattern is discerned at $x/H = 4.75$, showing the localized influence of the growing vortical structures. The global influence of the shedding large-scale vortical structures is seen from their regular light footprints near the rib edge ($x/H = 0.75$). In addition, the high-correlation zones along $fH/U_0 = 0.03$ at $x/H = -0.2$ demonstrate similar aspects of the quasi-deterministic vortical structures shedding along the elevated shear layer behind the rib. In addition, the flapping motion

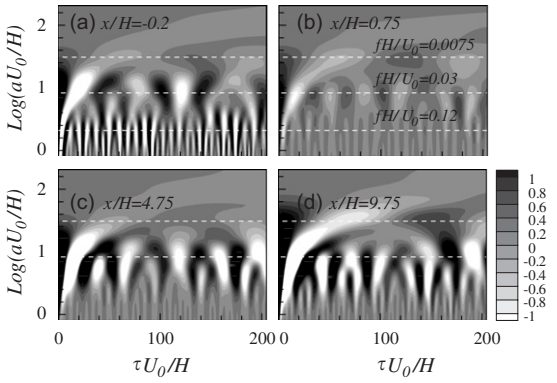

Fig. 9. Autocorrelation of continuous wavelet-transformed wall-pressure fluctuations at: (a) $x/H = -0.2$, (b) 0.75, (c) 9.75, and (d) 13.75.

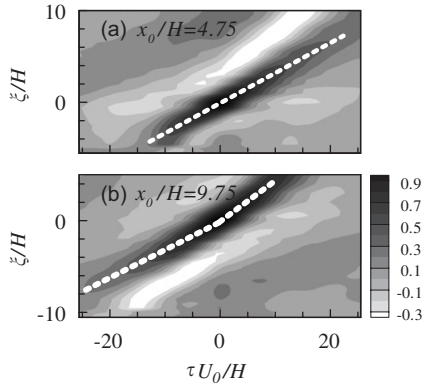

Fig. 10. Cross-correlation of wall-pressure fluctuations at: (a) $x_0/H = 4.75$ and (b) 9.75.

of the separation bubble at the low frequency of $fH/U_0 = 0.0075$ ($\log(aU_0/H) = 1.55$) is indicated by the corresponding signatures at $x/H = 0.75$ and 9.75, which gives rise to the sharp variation of the reverse-flow intermittency in the reattachment zone. However, the magnitude of the wavelet autocorrelation coefficients of the wall pressure along $fH/U_0 = 0.0075$ is relatively weak at $x/H = 4.75$ ($(x - x_R)/x_R = -0.51$) in Fig. 9(c), while in the separated and reattaching flow over a backward-facing step the peak wavelet correlation magnitude at the flapping frequency was clearly seen at $(x - x_R)/x_R = -0.45$ [Fig. 13 in Liu et al. (2005)]. These findings are consistent with the bidirectional shrinkage and enlargement of the separation bubble having little influence on the local wall-pressure fluctuations in the middle position of the separation bubble behind the rib, which is revisited in Fig. 17.

The convective features of the large-scale vortical structures were obtained by determining the cross-correlations of the wall-pressure field, the spatio-temporal variation of which was resolved by using the microphone array. The cross-correlation of the wall-pressure signals is defined as

$$\rho_{pp}(\xi, \tau; x_0) = \frac{\langle p'(x_0, t)p'(x_0 + \xi, t + \tau)\rangle}{\langle p'(x_0, t)p'(x_0, t)\rangle}. \tag{3}$$

Contour maps of the cross-correlation coefficients of the wall-pressure referenced at $x_0/H = 4.75$ and 9.75 are depicted in Fig. 10. Examination of Fig. 10 shows that there is a main ridge of positive correlation inclined at an angle and two negative zones on either side of this main ridge. From the slope of the main ridge, the average convection speeds of the vortical structures at $x_0/H = 4.75$ and 9.75 are calculated to be $0.35U_0$ and $0.45U_0$, respectively. This means that the convection velocity increases as the fluid flows downstream, consistent with previous findings for the separated and reattaching turbulent flows over backward- and forward-facing steps [see Table 1; Farabee and Casarella (1986); Heenan and Morrison (1998)] and a fence [see Table 1; Hudy et al. (2003)]. The spatial variation in convection velocities of the separated and reattaching flows over different surface irregularities is summarized in Table 1. Recall that the convection speed of the wall-pressure fluctuations, though regarded as being primarily influenced by the

shedding large-scale vortical structures, is still an integral measure containing contributions from various intermittent events superimposed in the shear layer. In the central part of the separation bubble ($x/H = 4.75$), although the large-scale vortical structures at $fH/U_0 = 0.03$ dominate, as shown in Fig. 9(c), the near-wall reversed flow, which peaks at $u/U_0 = -0.25$ (Fig. 5), reduces the convection speed which is determined by the local wall-pressure fluctuations. Downstream of the reattachment point, the large-scale vortical structures begin to decay and the wall-pressure fluctuations in the higher frequency range become stronger. Thus, the dispersed structures are more likely diffusive into higher speed regions of the redeveloping turbulent boundary layer (Lee and Sung, 2002), yielding an increased convection speed as shown in Fig. 10(b).

The unsteady flow behavior associated with the large-scale vortical structures and the separation bubble was further elucidated by synchronized measurements of the wall-pressure fluctuations and the velocity fluctuations. The conditional signal of the wall pressure at the reattachment point $x/H = 9.75$ was used to extract the shedding vortical structures and the flapping separation bubble. However, the intermittent nature of the vortical structures at a single measurement point is prone to being obscured by localized small-scale events, yielding a smearing of the wall-pressure fluctuations. Accordingly, to scrutinize the temporal signatures associated with the passing vortical structures and the flapping separation bubble at specific frequencies, multi-resolution analysis (MRA) using the Maximum Overlap Discrete Wavelet Transform (MODWT) (Percival and Walden, 2000) was applied to the wall-pressure fluctuations and the velocity fluctuations. MODWT is characterized as a zero-phase filter, showing its potential for analyzing instantaneous scale-variant signals, which is of considerable practical significance in detecting intermittent vortical events using arrayed sensors. Details regarding the fundamentals and procedures of the transformation can be found in Percival and Walden (2000) and Chun et al. (2006), respectively. Multi-resolution instantaneous signals of the wall pressure at $x/H = 9.75$ are plotted in Fig. 11. By using MRA, the original time-series signals are extracted to a series of

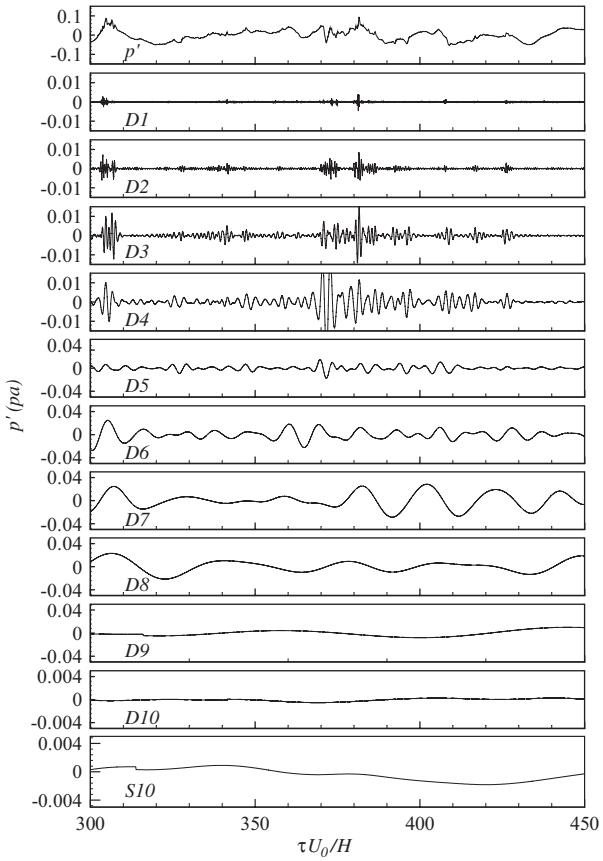

Fig. 11. Multi-resolution wall pressure at $x/H = 9.75$ by the MODWT. D1 ($fH/U_0 = 3.84$), D2 ($fH/U_0 = 1.92$), D3 ($fH/U_0 = 0.96$), D4 ($fH/U_0 = 0.48$), D5 ($fH/U_0 = 0.24$), D6 ($fH/U_0 = 0.12$), D7 ($fH/U_0 = 0.06$), D8 ($fH/U_0 = 0.03$), D9 ($fH/U_0 = 0.015$), D10 (0.0075), and S10 ($fH/U_0 \leqslant 0.0055$).

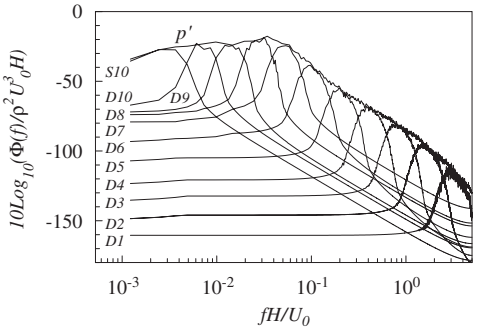

Fig. 12. Autospectra of the multi-resolution wall pressure at $x/H = 9.75$ by the MODWT. D1 ($fH/U_0 = 3.84$), D2 ($fH/U_0 = 1.92$), D3 ($fH/U_0 = 0.96$), D4 ($fH/U_0 = 0.48$), D5 ($fH/U_0 = 0.24$), D6 ($fH/U_0 = 0.12$), D7 ($fH/U_0 = 0.06$), D8 ($fH/U_0 = 0.03$), D9 ($fH/U_0 = 0.015$), D10 ($fH/U_0 = 0.0075$), and $S10$ ($fH/U_0 \leqslant 0.0055$).

band-passed details, D_n, $D_{n-1},\ldots,D_2,D_1$, at successively smaller central frequency levels, as well as the low-passed smooth part S_n (Chun et al., 2006). The central frequency related to each scale of the detailed part is successively halved with increasing the level, as can be seen in the autospectrum of the corresponding multi-resolution wall pressure shown in Fig. 12. In the present study, the signal at D8 corresponds to the central frequency of the large-scale vortical structures (i.e. $fH/U_0 = 0.03$), while the signal at D10 ($fH/U_0 = 0.0075$) shows the decomposed one at the flapping frequency of the separation bubble. Consequently, the signals at D9, D7, D6, D5, D4, D3, D2 and D1 show the decomposed wall-pressure centered at the higher harmonic frequencies $fH/U_0 = 0.015$, 0.06, 0.12, 0.24, 0.48, 0.96, 1.92 and 3.84, respectively. By removing the contributions from higher frequency structures, the unsteady footprints of the large-scale vortical structures and the flapping separation bubble can be extracted from the curves at D8 and D10, respectively. Thus, in the following discussion the multi-resolution instantaneous wall pressures at $x/H = 9.75$, or the band-passed details D8 and D10, are mainly utilized as conditional signals to extract a wealth of information associated with intermittent events such as the shedding of the large-scale vortical structures and flapping of the separation bubble.

The instantaneous aspects of the shedding of large-scale vortical structures were disclosed by examining the cross-correlation between the conditionally sampled velocity field and the multi-resolution instantaneous wall pressure $fH/U_0 = 0.03$ (D8) at $x/H = 9.75$. According to Kiya and Sasaki (1985), negative instantaneous peaks in the fluctuating wall pressure are associated with the passage of large-scale vortical structures, whereas positive peaks arise from the downward inrush of the free-stream vortices. Thus, negative-peak detection of the decomposed wall pressure was employed to conditionally average the simultaneously acquired streamwise velocity field. The cross-correlation between the wall pressure and the velocity field is defined as

$$\rho_{pu}(x,y,\tau) = \overline{p'(x_0,t)u'(x,y,t+\tau)}/(p'_{\mathrm{rms}}u'_{\mathrm{rms}}). \tag{4}$$

Five sequential snapshots of the cross-correlation coefficients with time delays of $\tau = -T/2$, $-T/4$, 0, $T/4$ and $T/2$ are displayed in Fig. 13, where T is the shedding period of the large-scale vortical structures. The condition $\tau = 0$ corresponds to the appearance of the negative peak in the wall pressure. Inspection of the cross-correlation coefficients in Fig. 13(c) reveals that the slanted zones of high negative correlation are signatures of the large-scale vortical structures, with the spatial variation of these negative high-correlation zones with increasing τ reflecting the convective motion of the large-scale vortical structures. From estimations of the streamwise displacements of the negative high-correlation zones within the regions of $x/H \leqslant 9.75$ and $x/H \geqslant 9.75$, we find that the convection speeds of the large-scale vortical structures before and after the reattachment point are $0.32U_0$ and $0.45U_0$, respectively. The position with the negative correlation peak at the near-wall region is denoted by an arrow in Fig. 13. As the fluid flows downstream, the negative high-correlation zone convects downstream; no clear downward motion of the negative high-correlation zone was detected, similar to the behavior reported previously for the separated and reattaching flow over a blunt body (Chun and Sung, 2003). However, the growth of the large-scale vortical structures is indicated by the expansion in size of the concentrated zone. At time $\tau = 0$ (Fig. 13(c)), the near-wall region at $x/H = 9.75$ is engulfed by the extended negative high-correlation zone, which is indicative of the significant influence of the large-scale vortical structures on the reattachment zone. As the large-scale vortical structures convect downstream of the reattachment position ($\tau = T/4$ and $T/2$), the streamwise length of the near-wall negative high-correlation zone is extended due to the decay of the large-scale vortical structures in the redeveloping turbulent boundary layer.

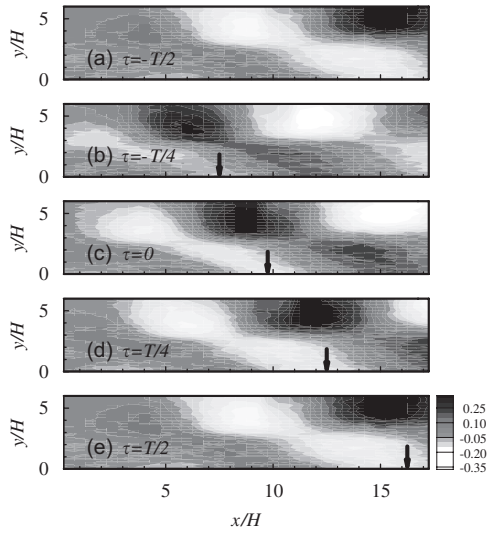

Fig. 13. Cross-correlation between the conditionally averaged wall pressure at $x/H = 9.75$ and the streamwise velocity component: (a) $\tau = -T/2$, (b) $-T/4$, (c) 0, (d) $T/4$, and (e) $T/2$.

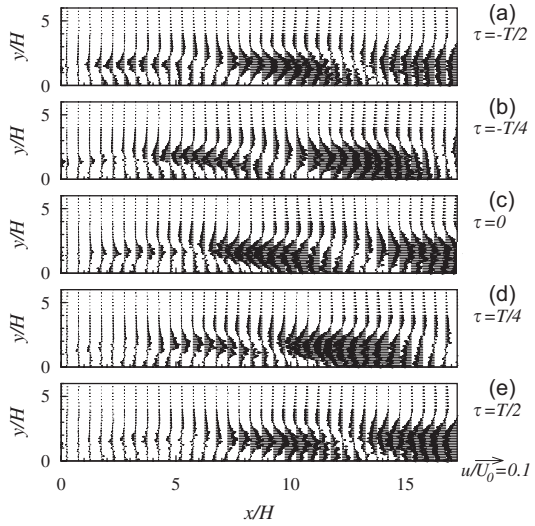

Fig. 14. Conditionally averaged streamwise velocity at D8 ($fH/U_0 = 0.03$) with subtraction of the local time-mean velocity: (a) $\tau = -T/2$, (b) $-T/4$, (c) 0, (d) $T/4$, and (e) $T/2$.

Further understanding of the convective motion of the shedding large-scale vortical structures was obtained from the conditionally averaged streamwise velocity field shown in Fig. 14. The local time-mean velocity was subtracted from the conditionally averaged velocity, allowing close examination of the internal structure of the spatially evolving vortices. Comparison of Figs. 13 and 14 discloses that the backflow velocity at $\tau = 0$ is highest at $x/H = 9.75$, consistent with the reattachment of the large-scale vortical structures. Inspection of the backflow traces at $\tau = -T/2$, $-T/4$ and 0 demonstrates the growing strength of the large-scale vortical structures in the separated turbulent flow, while in the downstream region intensification of the streamwise velocity component of the vortical structures (Fig. 14(d)) is caused by its strong impingement onto the wall. As the large-scale vortical structures convect downstream (Fig. 14(e)), the streamwise velocity component of the vortical structures decreases due to its decay.

In the foregoing discussion, the large-scale vortical structures shedding at the frequency D8 ($fH/U_0 = 0.03$) were scrutinized. Now we turn to the low-frequency flapping motion of the separation bubble, which has been widely observed in the separated and reattaching turbulent flows over a backward-facing step (Eaton and Johnston, 1981; Lee

and Sung, 2002) and a blunt body (Kiya and Sasaki, 1985). The positive-peak wall pressure at the flapping frequency D10 corresponds to the extreme shrinkage phase of the separation bubble (Lee and Sung, 2002). The phase relationship between the decomposed wall pressure D10 ($fH/U_0 = 0.0075$) at $x/H = 9.75$ and the instantaneous reverse-flow intermittency at $x/H = 9.75$ and $y/H = 0.05$ is schematically illustrated in Fig. 15. As shown in Fig. 15, the zero-pressure condition coincides with the phase $\gamma_t = 0.5$. Recall that the flapping motion of the separation bubble is composed of enlargement and shrinkage states (Lee and Sung, 2002). When the separation bubble is in the enlargement state ($0 \leqslant \tau U_0/H \leqslant 66$), the shear layer moves downstream and upwards, reducing the wall pressure in the reattachment zone. The shrinkage motion of the separation bubble ($-66 \leqslant \tau U_0/H < 0$), by contrast, gives rise to an increase in the wall pressure in the reattachment zone.

An in-depth impression of the flapping motion of the separation bubble was gained by determining the time-dependent reattachment position. Positive-peak detection of the multi-resolution wall pressure $fH/U_0 = 0.0075$ at the time-averaged reattachment point $x/H = 9.75$ was employed to conditionally sample the near-wall streamwise velocity along the streamwise stations ($y/H = 0.05$). At each streamwise station, the near-wall flow reversal in phase with the flapping motion was calculated statistically. By using the reverse-flow intermittency factor $\gamma_t = 0.5$, the instantaneous reattachment length of the separated flow was obtained, which is closely related to the flapping motion. The time-dependent streamwise positions with $\gamma_t = 0.5$ in one period of the flapping motion are displayed in Fig. 16. It is evident that the variation of the reattachment point with time shows a wave-like distribution centered at the time-averaged reattachment point $9.75H$. The streamwise length of the reattaching zone is determined to be $1.2H$, a narrow region compared with that of the separated and reattaching turbulent flow over a backward-facing step (Eaton and Johnston, 1981). The shorter reattaching zone of the rib system can be attributed to the elevation of the separated shear layer in this system, as well as the involvement of the reverse flow above the rib in the bidirectional enlargement and shrinkage states of the separation bubble. The latter aspect is revisited in our discussion of Fig. 17.

Finally, to elucidate the influence of the flapping motion of the separation bubble on the separated and reattaching turbulent flow, we examined conditional averages of the reverse-flow intermittency at the near-wall region at various streamwise stations. The measurement position was $y/H = 0.05$ for the stations upstream ($x/H < -1$) and downstream ($x/H > 0$) of the rib, and $y/H = 1.05$ for the stations on top of the rib ($-1 < x/H < 0$). The variation of the reverse-flow intermittency in one period of the flapping motion is plotted in Fig. 17 as a function of the streamwise coordinate x/H. In the bulk region of the separation bubble ($1.0 \leqslant x/H \leqslant 8.0$), the reverse-flow intermittency is greater than 0.5, indicating comparatively stable reverse flow. In the region $9.0 \leqslant x/H \leqslant 10.25$, the reverse-flow intermittency undergoes large variations, indicative of highly unstable flow. This is attributed to the strong interaction between the flapping separation bubble and the reattaching large-scale vortical structures (Kiya and Sasaki, 1985). The prominent large variation of the reverse-flow intermittency at $x/H = 0.75$ can be attributed to the strongly fluctuating interface between

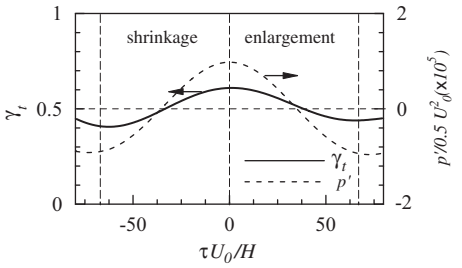

Fig. 15. Illustration of the phase relationship between the varying reverse-flow intermittency ($x/H = 9.75$, $y/H = 0.05$) and the instantaneous wall pressure at $x/H = 9.75$ (D10, $fH/U_0 = 0.0075$).

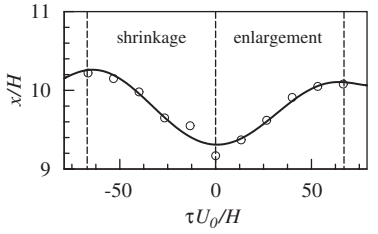

Fig. 16. Time-dependent reattachment point in one period of the flapping motion at D10 ($fH/U_0 = 0.0075$).

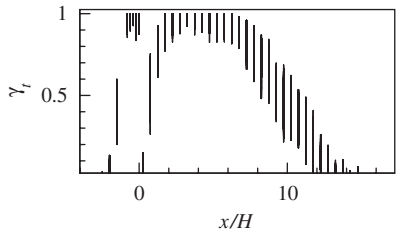

Fig. 17. Variation of the conditionally averaged reverse-flow intermittency in one period of the flapping motion ($fH/U_0 = 0.0075$) at various streamwise stations.

the separation bubble and the corner flow, where the near-wall flow behavior is significantly influenced by the flapping separation bubble. Furthermore, the variation of the reverse-flow intermittency above the rib is similar in scale to that in the central region of the separation bubble ($2.25 \leqslant x/H \leqslant 6.25$), suggesting that the reverse flow on the rib is not immune to the flapping motion of the separation bubble.

4. Conclusions

In the present study, the spatio-temporal characteristics of the separated and reattaching turbulent flow over a two-dimensional square rib were investigated experimentally, with particular focus on the shedding large-scale vortical structures and the flapping separation bubble downstream of the rib. To elucidate the flow characteristics, high-quality synchronized measurements of the wall-pressure fluctuations and the velocity fluctuations were made using a microphone array and a split-fiber film, respectively. Profiles of the time-averaged streamwise velocity and the wall-pressure fluctuation coefficient showed that the shear layer separated from the leading edge of the rib sweeps past the rib and directly reattaches on the bottom wall ($x/H = 9.75$) downstream of the rib, and that a thin layer of reverse flow is formed above the rib. Features corresponding to the shedding large-scale vortical structures ($fH/U_0 = 0.03$) and the flapping separation bubble ($fH/U_0 = 0.0075$) were detected in the wall-pressure spectra and the autocorrelation of the continuous wavelet transformed wall pressure. From the cross-correlation of the wall-pressure fluctuations, the convection speeds of the large-scale vortical structures before and after the reattachment point were found to be $U_c = 0.35U_0$ and $0.45U_0$, respectively. The cross-correlation between the multi-resolution wall pressure ($fH/U_0 = 0.03$) at the time-averaged reattachment point $x/H = 9.75$ and the streamwise velocity field convincingly showed the convection, growth and decay of the large-scale vortical structures. The influence of the flapping separation bubble on the turbulent flow was analyzed in terms of the conditionally averaged reverse-flow intermittency. The wave-like phase relationship between the varying reattachment length and the instantaneous wall pressure ($fH/U_0 = 0.0075$) decomposed by using MODWT was observed, showing the streamwise length $1.2H$ of the reattachment zone centered at $x/H = 9.75$. The variation of the conditionally averaged reverse-flow intermittency in one period of the flapping motion at various streamwise stations demonstrated the presence of strongly unstable flow in the reattachment zone and the interfacial area between the separation bubble and the corner flow. In addition, the thin reverse flow above the rib was found to be influenced by the flapping motion of the separation bubble behind the rib.

Acknowledgment

This work was supported by a grant (no. 50606024) from the national Natural Science Foundation of China (NSFC).

References

Acharya, S., Dutta, S., Myrum, T.A., Baker, R.S., 1994. Turbulent flow past a surface-mounted two-dimensional rib. ASME Journal of Fluids Engineering 116, 238–246.

Antoniou, J., Bergeles, G., 1988. Development of the reattachment flow behind surface-mounted two-dimensional prisms. ASME Journal of Fluids Engineering 110, 127–133.

Bergeles, G., Athanassiadis, N., 1983. The flow past a surface-mounted obstacle. ASME Journal of Fluids Engineering 105, 461–463.

Brederode, V., Bradshaw, P., 1978. Influence of the side walls on the turbulent center-plane boundary-layer in a square duct. ASME Journal of Fluids Engineering 100, 91–96.

Castro, I.P., 1979. Relaxing wakes behind surface-mounted obstacles in rough wall boundary layers. Journal of Fluid Mechanics 93, 631–659.

Chun, K.B., Sung, H.J., 1996. Control of turbulent separated flow over a backward-facing step by local forcing. Experiments in Fluids 21, 417–426.

Chun, S., Sung, H.J., 2003. Large-scale vortical structure of turbulent separated bubble affected by unsteady wake. Experiments in Fluids 34, 572–584.

Chun, S.J., Liu, Y.Z., Sung, H.J., 2004. Wall pressure fluctuations of a turbulent separated and reattaching flow affected by an unsteady wake. Experiments in Fluids 37, 531–546.

Chun, S.J., Liu, Y.Z., Sung, H.J., 2006. Multi-resolution analysis of the large-scale coherent structure in a turbulent separation bubble affected by unsteady wake. Journal of Fluids and Structures 23, 85–100.

Eaton, J.K., Johnston, J.P., 1981. A review of research on subsonic turbulent flow reattachment. AIAA Journal 19, 1093–1100.

Farabee, T.M., Casarella, M.J., 1986. Measurement of fluctuating wall pressure for separated/reattached boundary flows. Journal of Vibration, Acoustics, Stress and Reliability in Design 108, 301–307.

Heenan, A.F., Morrison, J.F., 1998. Passive control of pressure fluctuations generated by separated flow. AIAA Journal 36, 1014–1022.

Hudy, L.M., Naguib, A.M., Humphreys, W.M., 2003. Wall pressure-array measurements beneath a separating/reattaching flow region. Physics of Fluids 15, 706–717.

Hwang, R.R., Chow, Y.C., Peng, Y.F., 1999. Numerical study of turbulent flow over two-dimensional surface-mounted ribs in a channel. International Journal of Numerical Methods in Fluids 31, 767–785.

Kiya, M., Sasaki, K., 1985. Structure of large-scale vortices and unsteady reverse flow in the reattaching zone of a turbulent separation bubble. Journal of Fluid Mechanics 154, 463–491.

Lee, I., Sung, H.J., 2002. Multiple-arrayed pressure measurement for investigation of the unsteady flow structure of a reattaching shear layer. Journal of Fluid Mechanics 463, 377–402.

Li, H., 1998. Identification of coherent structure in turbulent shear flow with wavelet correlation analysis. ASME Journal of Fluids Engineering 120, 778–785.

Liu, Y.Z., Kang, W., Sung, H.J., 2005. Assessment of the organization of a turbulent separated and reattaching flow by measuring wall pressure fluctuations. Experiments in Fluids 38, 485–493.

Liu, Y.Z., Ke, F., Chen, H.P., Sung, H.J., 2006. A wall-bounded turbulent mixing layer flow over an open step. Part 1: Time-mean and spectral characteristics. Journal of Turbulence 7, 1–17.

Liu, Y.Z., Ke, F., Chen, H.P., Sung, H.J., 2007. A wall-bounded turbulent mixing layer flow over an open step. Part 2: Unsteady characteristics. Journal of Turbulence 8, 1–17.

Murata, A., Mochizuki, S., 2000. Large eddy simulation with a dynamic subgrid-scale model of turbulent heat transfer in an orthogonally rotating rectangular duct with transverse rib turbulators. International Journal of Heat and Mass Transfer 43, 1243–1259.

Panigrahi, P.K., Acharya, S., 1996. Spectral characteristics of separated flow behind a surface-mounted square rib. AIAA Journal 96-1931, 1–8.

Panigrahi, P.K., Acharya, S., 2004. Multi-modal forcing of the turbulent separated shear flow past a rib. ASME Journal of Fluids Engineering 126, 22–31.

Percival, D.B., Walden, A.T., 2000. Wavelet Methods for Time Series Analysis. Cambridge University Press, Cambridge.

Roos, F.W., Kegelman, J.T., 1986. Control of coherent structures in reattaching laminar and turbulent shear layer. AIAA Journal 24, 1956–1963.

Saha, A.K., Acharya, S., 2005. Unsteady RANS simulation of turbulent flow and heat transfer in ribbed coolant passages of different aspect ratios. International Journal of Heat and Mass Transfer 48, 4704–4725.

Tropea, C.D., Gackstatter, R., 1985. The flow over two-dimensional surface-mounted obstacles at low Reynolds numbers. ASME Journal of Fluids Engineering 107, 489–494.

Wood, D.H., Bradshaw, P., 1982. A turbulent mixing layer constrained by a solid surface. Part 1: measurements before reaching the surface. Journal of Fluid Mechanics 122, 57–58.